AGU PUBLICATIONS

JGR

Journal of Geophysical Research: Atmospheres

RESEARCH ARTICLE
10.1002/2014JD022234

Key Points:
- High-resolution field campaign was conducted in the East China Sea
- Small-scale sea surface temperature variations influence Baiu frontal zone
- Evaporation from Kuroshio has a remote impact on Baiu frontal zone

Correspondence to:
A. Manda,
manda@nagasaki-u.ac.jp

Citation:
Kunoki, S., et al. (2015), Oceanic influence on the Baiu frontal zone in the East China Sea, *J. Geophys. Res. Atmos.*, *120*, doi:10.1002/2014JD022234.

Received 27 JUN 2014
Accepted 11 DEC 2014
Accepted article online 17 DEC 2014

Oceanic influence on the Baiu frontal zone in the East China Sea

Shiori Kunoki[1,2], Atsuyoshi Manda[3], Yasu-Masa Kodama[1], Satoshi Iizuka[4], Kazutoshi Sato[1], Ibnu Fathrio[1], Taku Mitsui[3], Hiromu Seko[5], Qoosaku Moteki[6], Shoshiro Minobe[7], and Yoshihiro Tachibana[8]

[1]Department of Earth and Environmental Sciences, Graduate School of Science and Technology, Hirosaki University, Hirosaki, Japan, [2]PASCO CORPORATION, Tokyo, Japan, [3]Graduate School of Fisheries Science and Environmental Studies, Nagasaki University, Nagasaki, Japan, [4]Monitoring and Forecast Research Department, National Research Institute for Earth Science and Disaster Prevention, Tsukuba, Japan, [5]Meteorological Research Institute, Japan Meteorological Agency, Tsukuba, Japan, [6]Department of Coupled Ocean-Atmosphere-Land Processes Research, Japan Agency for Marine-Earth Science and Technology, Yokosuka, Japan, [7]Graduate School of Science, Hokkaido University, Sapporo, Japan, [8]Climate and Ecosystem Dynamics Division, Mie University, Tsu, Japan

Abstract A high-resolution transect of atmospheric soundings across the Kuroshio Current in the East China Sea was conducted onboard a ship in June 2012 with the objective of analyzing the influence of the complex sea surface temperature (SST) distribution on the Baiu frontal zone (BFZ). Expendable bathythermograph castings and continuous surface meteorological observations were also examined. Two distinct mesoscale atmospheric fronts, characterized by changes of wind direction in the lower troposphere and surface air temperature, were found in the BFZ. One (northern) atmospheric front was observed around the SST front in relation to a warm water tongue extending from the Kuroshio. A high SST region around the northern atmospheric front enhances unstable near surface stratification and intensifies turbulent heat flux. They help modify the marine atmospheric boundary layer in the BFZ. The other (southern) atmospheric front was at the southern end of the BFZ. Intense evaporation over the Kuroshio and moisture transport by southerly winds were important in forming the conditionally unstable air masses in the lower troposphere of the BFZ.

1. Introduction

The Baiu frontal zone (BFZ) is a quasi-stationary precipitation region occurring over East Asia and the northwestern Pacific typically in early summer, between June and July [e.g., *Akiyama*, 1973; *Chen and Chang*, 1980; *Kodama*, 1992; *Ding and Chen*, 2005; *Ninomiya and Shibagaki*, 2007]. The BFZ displays large variability on time scales from hours to interannual, making it perhaps the single most important climatic phenomenon in East Asia [*Sampe and Xie*, 2010]. The BFZ is accompanied by characteristic frontal structures in the lower troposphere, which together are called the Baiu front, and can be identified by sharp gradients of specific humidity and equivalent potential temperature [*Ninomiya*, 1984] and a horizontal wind shear line [*Akiyama*, 1973]. The front shows multiscale structures from meso to synoptic, and interactions among various timescales are believed to be essential to develop and maintain the BFZ [*Ninomiya and Akiyama*, 1992; *Moteki et al.*, 2004a, 2004b]. Mesoscale disturbances frequently develop within the BFZ, accompanied by intense convection and heavy rain, occasionally causing flooding and mudslides [e.g., *Ogura et al.*, 1985; *Kato*, 1998; *Davidson et al.*, 1998; *Ninomiya and Shibagaki*, 2007; *Maeda et al.*, 2008; *Manda et al.*, 2014].

The BFZ in the East China Sea (ECS) has features different from those east of Japan. In contrast to the latter which is accompanied by a strong meridional gradient of both humidity and temperature, the BFZ in the ECS is characterized by a pronounced meridional gradient of humidity rather than of temperature [*Ninomiya*, 1984]. *Kato et al.* [2003] proposed a conceptual model of the BFZ in the ECS (see Figure 5 of their paper), which goes as follows: The BFZ corresponds to a region with a moist tongue extending from the continent of China or the ECS to western Japan. In the lower troposphere, there is a southerly flow into the BFZ, which forms a thin layer of warm and humid air. The thickness of this layer is approximately 1.5 km. Above this is a relatively dry layer, attributable to subsidence from the Pacific high. There are dry and cold air masses north of the BFZ, where westerly flow is predominant.

The complex structure of sea surface temperature (SST) in the ECS can affect many important atmospheric phenomena on various time scales. *Xie et al.* [2002] showed that a sharp SST front near the Kuroshio Current had a significant impact on the development of a mesoscale low-pressure system in the ECS during winter. *Miyama et al.* [2012] reported that high SST in the Kuroshio helped organize and maintain a well-defined convective rainband in May. *Xu et al.* [2011] showed that a spring Kuroshio front in the ECS influenced both boundary layer convergence and deep cumulus convection.

Recent studies have pointed out the effects of SST variation in the ECS on the Baiu front. *Moteki and Manda* [2013] revealed a close relationship between seasonal migrations of the BFZ and SST on both climatological and synoptic timescales, suggesting the importance of surface heat fluxes over the ECS in seasonal migrations of the Baiu front. *Kuwano-Yoshida et al.* [2013] demonstrated that surface evaporation over the warm ocean current was important for maintenance of the quasi-stationary BFZ. *Sasaki et al.* [2012] reported that strong surface evaporation and surface convergence associated with the local SST maximum along the Kuroshio strengthened Baiu precipitation over the ECS, indicating that this warm SST region has a significant impact on precipitation systems in the ECS. *Manda et al.* [2014] showed through a suite of numerical experiments that intensified evaporation due to a rapid rise in SST during early summer over the ECS augmented water vapor content in the lower troposphere and helped maintain the convectively unstable conditions of warm and humid air masses from the tropics. They concluded that these conditions were one of the main contributors to the torrential rainfall events during Baiu rainy season (typically from June to mid-July) in the western part of Japan.

Tanimoto et al. [2009] carried out an atmospheric sounding campaign similar to the present study to illustrate Kuroshio-Baiu interaction at the Kuroshio Extension (KE) in the northwestern Pacific, east of Japan. They found that surface heat flux over the KE influenced the marine atmospheric boundary layer (MABL) and fog/low-cloud formation. However, in situ atmospheric vertical soundings in the ECS, where the BFZ has features different from those in the KE, have been lacking. Thus, most studies of Kuroshio-Baiu interaction in the ECS have been based on models or model-assimilation analyses, hampering progress in characterizing and understanding the Kuroshio influence on the BFZ in the ECS. This paper focuses on the impact of SST distributions around the Kuroshio on the BFZ in the ECS. SST influence in the extratropics is of modest amplitude relative to internal atmospheric variability and is difficult to detect [*Kushnir et al.*, 2002]. We therefore made high-resolution atmospheric soundings, since relatively weak signals of midlatitude air-sea interaction are most detectable for phenomena whose spatial scales are of the same order as that of the SST fronts [*Minobe et al.*, 2015]. A sampling interval of ~20 km was chosen so that atmospheric and oceanic phenomena with horizontal scale of SST fronts near the Kuroshio in the ECS (~100 km) could be resolved. To our knowledge, such high-resolution soundings targeting the Kuroshio-Baiu interaction in the ECS have been extremely limited. Our study cruise thus offered an excellent opportunity to deepen understanding of the nature of that interaction.

During the cruise, we observed two distinct frontal structures in the BFZ similar to the frontal structures reported by *Moteki et al.* [2004a, 2004b, 2006]. However, their analyses were limited to atmospheric data and they did not investigate oceanic influences on frontal structures of the BFZ. In contrast to these previous studies, the present work highlights the overlooked critical importance of oceanic influences on the BFZ. One (northern) atmospheric front was observed around the SST front caused by a warm water tongue extending from the Kuroshio. A high SST region around the northern atmospheric front enhanced unstable near surface stratification and intensified turbulent heat flux. They helped modify the marine atmospheric boundary layer. The other (southern) atmospheric front was at the southern end of the BFZ. Intense evaporation over the Kuroshio water and moisture transport from the water were found to be important contributors to water vapor content and stability in the lower troposphere of the BFZ.

The rest of the paper is organized as follows. Section 2 describes the field campaign and data. Section 3 depicts synoptic atmospheric conditions and evolution of the precipitation system associated with BFZ during the period of the campaign. Section 4 describes the frontal structures in the BFZ observed during the campaign. Section 5 discusses the oceanic influences on the BFZ. In particular, the influence of complex SST distribution on the MABL structure and the importance of moisture supply from the Kuroshio to the water vapor content and atmospheric stability in the lower troposphere of the BFZ are discussed. Section 6 presents a summary and discussion.

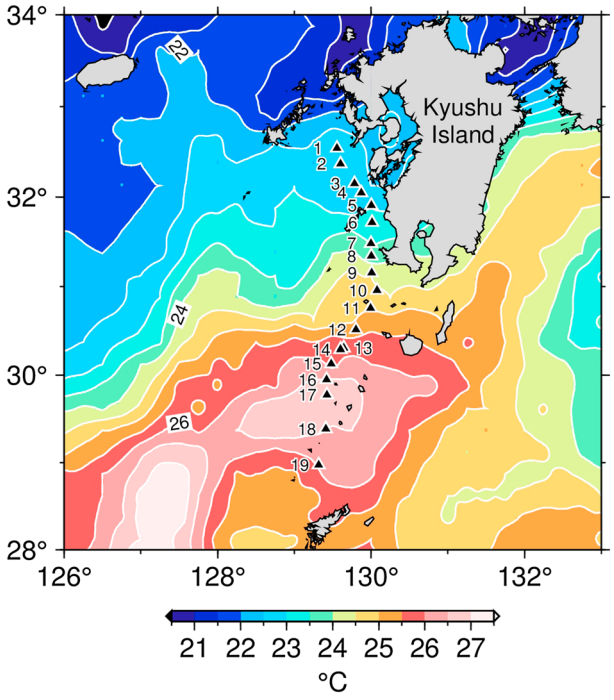

Figure 1. Map of study area. Triangles indicate locations of GPS sonde stations and XBT casting sites. Numerals beside triangles indicate station numbers. Color shading and contours indicate MGDSST (°C) on 15 June 2012.

2. Observation and Data

A joint survey of the ECS ocean-atmosphere system was conducted in June 2012 onboard the training vessel (T/V) *Nagasaki-Maru* of Nagasaki University, as part of the project "Hot Spot in Climate System: Coupled Ocean-Atmosphere Variability over Monsoonal Asia due to Contiguousness Between Tropical Warmness and Arctic Coolness." The project was led by Prof. Hisashi Nakamura of the University of Tokyo. The present study focuses on a nearly meridional transect of atmospheric soundings across the Kuroshio for illustrating the Kuroshio-Baiu interaction. Figure 1 shows sounding stations (triangles) along the transect, overlaid on concurrent SST fields (color shading and contours). Time and geographical coordinates of the soundings and castings are shown in Table 1. Onboard the ship, we used global positioning system (GPS) sondes (Meisei RS-06G) to measure air temperature, relative humidity (RH), and wind velocity every 1 s from the sea surface to ~10 km in the lower stratosphere. We also used expendable bathythermographs (XBT; Tsurumi T7) to measure sea water temperature from the surface to depth 760 m. Surface marine meteorological observations of SST, surface air temperature (SAT), surface wind velocity, and RH were available at 1 min intervals.

To supplement the field data campaign, the following oceanic and atmospheric data sets were used in this study. Merged satellite and in situ data Global Daily Sea Surface Temperature (MGDSST) furnished by the

Table 1. Date/Time and Geographical Coordinates of GPS Sonde Soundings and XBT Castings

Station	Date	Time (UTC)	Latitude (N)	Longitude (E)
1	6/15/2012	02:31	32°32′29″	129°36′25″
2	6/15/2012	03:29	32°22′03″	129°39′14″
3	6/15/2012	04:50	32°09′07″	129°50′10″
4	6/15/2012	05:31	32°02′52″	129°55′16″
5	6/15/2012	06:26	31°54′25″	130°03′22″
6	6/15/2012	07:27	31°43′13″	130°03′43″
7	6/15/2012	08:42	31°29′11″	130°03′00″
8	6/15/2012	09:28	31°20′36″	130°03′11″
9	6/15/2012	10:27	31°09′21″	130°03′29″
10	6/15/2012	11:25	30°57′39″	130°04′23″
11	6/15/2012	12:30	30°45′23″	130°02′35″
12	6/15/2012	13:30	30°30′59″	129°51′18″
13	6/15/2012	14:57	30°18′29″	129°41′46″
14	6/15/2012	15:30	30°17′37″	129°39′11″
15	6/15/2012	16:30	30°07′59″	129°31′55″
16	6/15/2012	17:30	29°57′17″	129°28′19″
17	6/15/2012	18:26	29°46′47″	129°28′23″
18	6/15/2012	20:38	29°23′26″	129°27′47″
19	6/15/2012	22:23	28°58′37″	129°22′12″

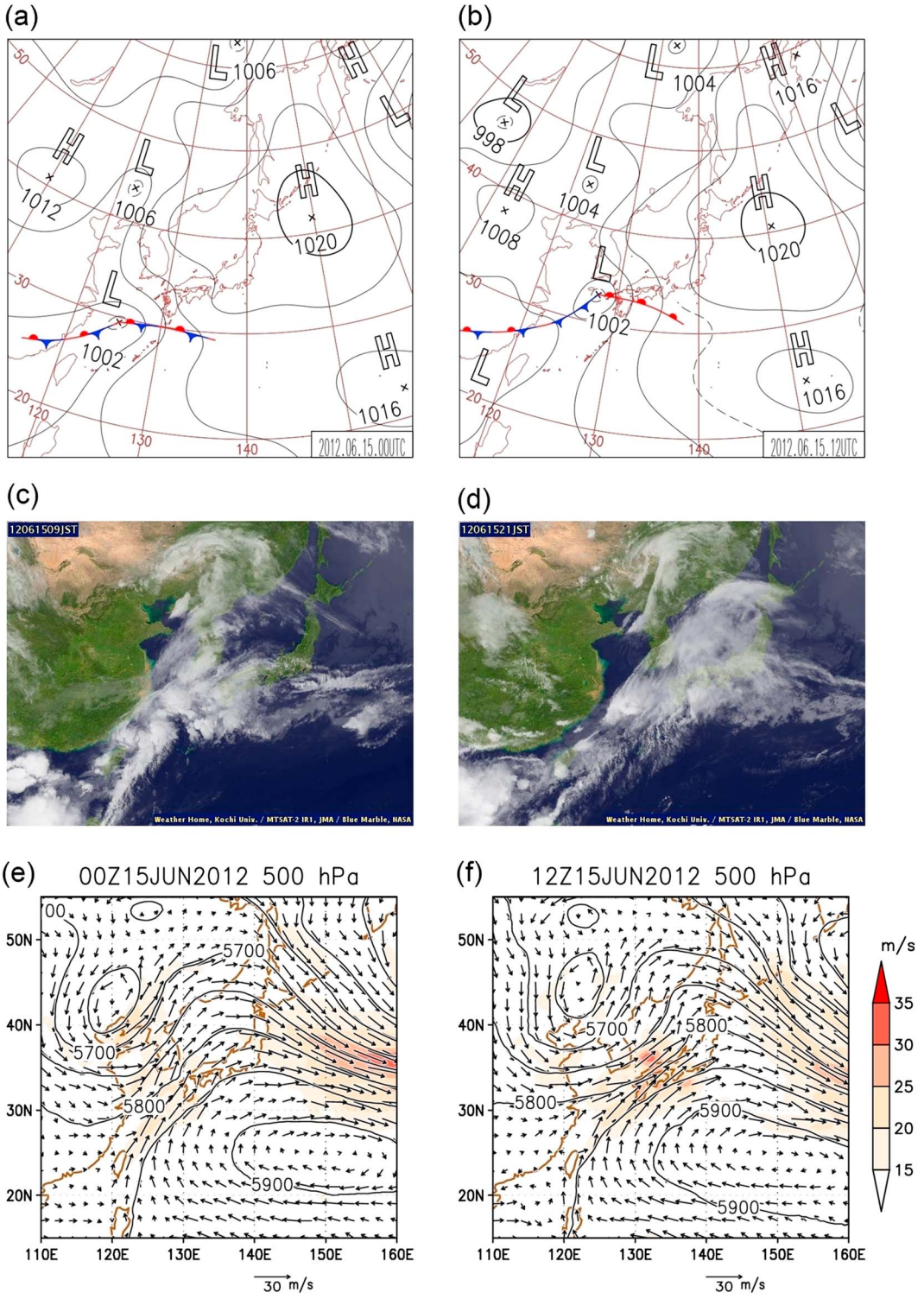

Figure 2. Surface weather maps at (a) 0000 and (b) 1200 UTC on 15 June 2012. Infrared images from the Multi-functional Transport Satellite-2 (MTSAT-2) at (c) 0000 and (d) 1200 UTC on 15 June 2012. Horizontal wind field (vector), wind speed (color), and geopotential height in meters (contour) of the GSM output at (e) 0000 and (f) 1200 UTC on 15 June 2012. All the maps, images, and data were provided by Japan Meteorological Agency.

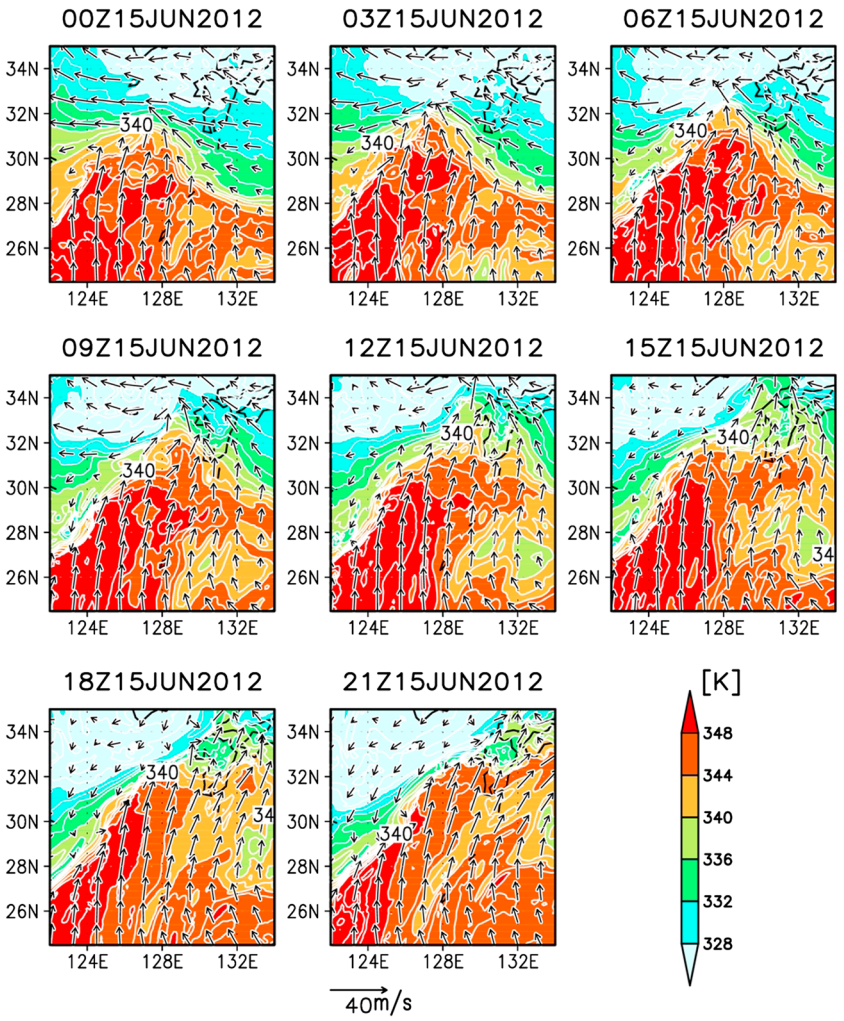

Figure 3. Snapshots of horizontal wind field (vectors) and equivalent potential temperature (color shade and contours) of M-ANAL at 950 hPa level.

Japan Meteorological Agency (JMA) were used, as well as SST data estimated by the Japan Coastal Ocean Predictability Experiment 2 (JCOPE2) high-resolution ocean reanalysis system. This system was developed by the Japan Agency for Marine-Earth Science and Technology [*Miyazawa et al.*, 2009]. The JCOPE2 system assimilates satellite-derived sea surface height and SST data plus in situ temperature and salinity to reproduce the ocean state as accurately as possible. Horizontal resolution of JCOPE2 is 1/12°, much finer than that of MGDSST (1/4°). We used the mesoscale operational weather analysis (M-ANAL) for the Far East (20°–50°N, 120°–150°E) provided by the JMA. This analysis included tropospheric wind velocity, temperature, and RH (surface, 975, 950, 925, 900, 800, 700, 600, and 500 hPa), available at 3 h intervals on a 0.1° latitude × 0.125° longitude grid. MGDSST data are used for the bottom boundary condition in the M-ANAL system. Sounding data from the cruise were not assimilated in the M-ANAL system. As well as the M-ANAL, the outputs of Global Spectral Model (GSM) of the JMA were employed. Surface weather maps, satellite infrared images from the Multi-functional Transport Satellite-2, and gridded hourly precipitation data sets were provided by the JMA. The precipitation data sets were calibrated using rain gauge measurements. These data were used to depict synoptic weather conditions and spatiotemporal evolution of precipitation systems during the sounding campaign.

Surface turbulent heat fluxes are important parameters for assessing the oceanic influence on the atmosphere. Latent and sensible heat fluxes were estimated by using bulk aerodynamic formula [*Kondo*, 1975] in this study.

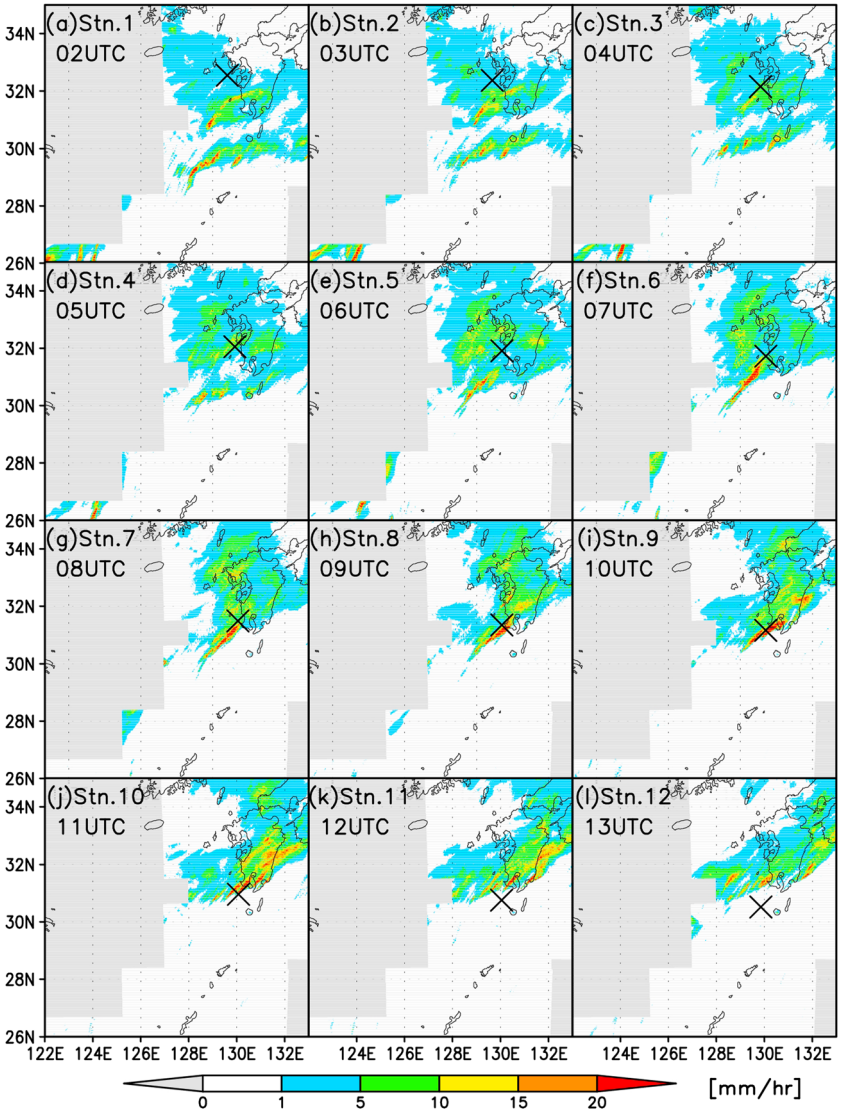

Figure 4. Hourly precipitation (color) measured by JMA radar (mm h^{-1}) at 1 h intervals. (a–l) 02–13 UTC on 15 June. Locations of atmospheric soundings are shown by crosses. Gray shading indicates area of unavailable precipitation data.

3. Synoptic Weather Conditions and Evolution of Precipitation Systems

Before examining the frontal structures in the BFZ and oceanic influence on the BFZ in later sections, this section is devoted to describe the synoptic weather conditions that characterize the environment of the frontal structures. Spatiotemporal evolution of precipitation systems that are important components of the BFZ is also portrayed. Figures 2a and 2b display a sequence of JMA surface weather maps showing locations of the Baiu front and surface pressure distributions during the sounding campaign. At 0000 UTC on 15 June 2012, the Baiu front accompanied by a weak mesolow centered at 30°N, 125°E stretched across the ECS, from the eastern coast of China through Japan and into the western North Pacific (Figure 2a). The low-pressure center then moved northeastward at 1200 UTC, with cold and warm fronts in its western and eastern portions, respectively (Figure 2b). As displayed in the satellite infrared images (Figure 2), the transect was overlaid by high-level clouds extending eastward and southwestward from the mesolow (Figure 2c). The cloud then stretched from southwest to northeast relative to the center of the mesolow (Figure 2d). In the middle troposphere, the GSM data indicated the presence of a high pressure system centered around 25°N, 150°E and trough over the Chinese continent (Figure 3e). Southwesterlies with local wind speed maxima

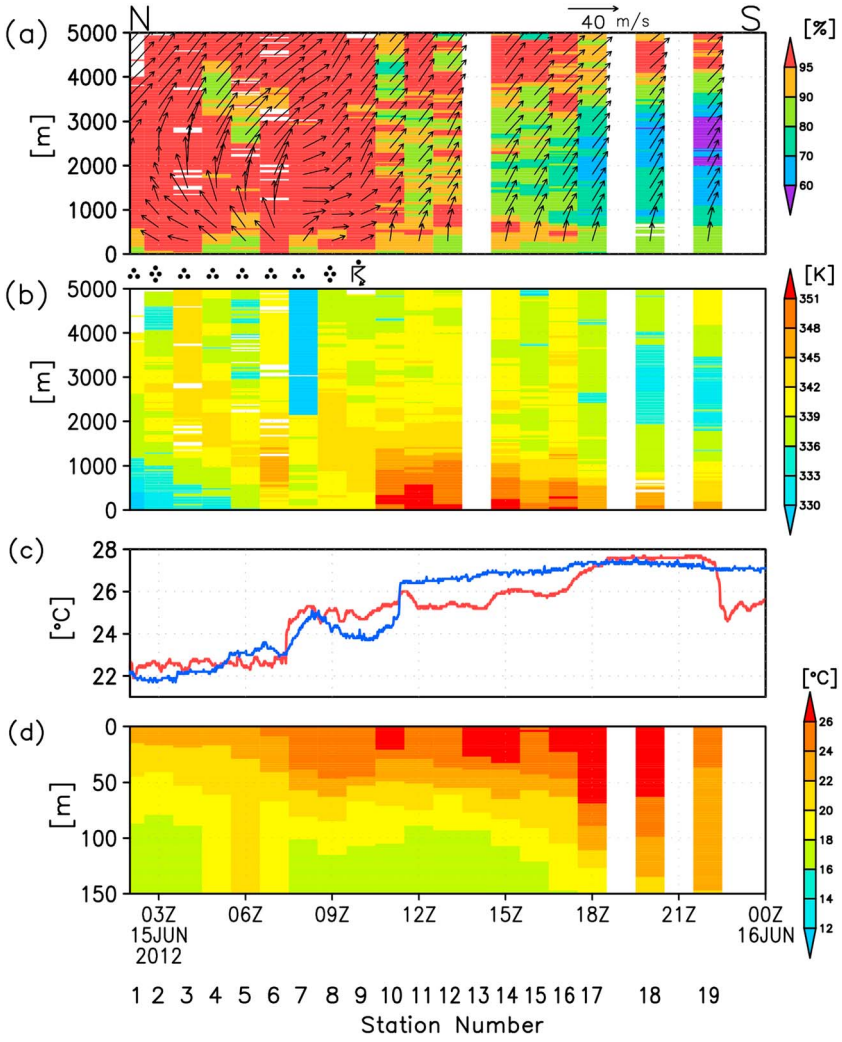

Figure 5. Atmospheric and oceanic fields observed during the field campaign. (a) Time-height cross sections of relative humidity (color) in percent and horizontal wind (vectors). Vectors directed downward denote northerlies. Weather marks shown at the bottom of Figure 5a are based on the field notes during the campaign. (b) Time-height cross sections of equivalent potential temperature in K from GPS sonde observations. (c) Time series of SST (red) and SAT (blue) in degree Celcius. (d) Time-depth cross section of water temperature in degree Celcius.

appeared between the high and trough over Kyushu Island (see Figure 1 for its location). The southwesterlies intensified at 1200 UTC and the location of the local maxima moved northeastward (Figure 3f).

Figure 3 shows horizontal distributions of equivalent potential temperature (EPT) and horizontal winds at 950 hPa level estimated by M-ANAL. The EPT front that was able to be discernible by contours of 340 K located south of Kyushu Island. Southerlies with warm and humid air dominated south of the EPT front. This prefrontal warm moist southerly flow is typical during Baiu rainy season in the ECS. The easterlies dominated north of the EPT front at 0000 UTC, and then wind gradually changed its direction and weakened as the EPT front migrates northward.

Figure 4 shows snapshots of hourly precipitation from 0200 to 1300 UTC on 15 June, superimposed on ship locations (crosses). A mesoscale precipitation system, indicated by the region where precipitation amount exceeded 1 mm h^{-1} with moderate to intense precipitation bands (10–20 mm h^{-1}), developed around Kyushu Island during the sounding campaign. The ship crossed these precipitation bands from 0200 to 1000 UTC (Figures 4a–4i) and traversed the southern end of the precipitation system between 1000 and 1100 UTC (Figures 4i and 4j), consistent with our field notes depicted by weather symbols shown at the bottom of Figure 5a.

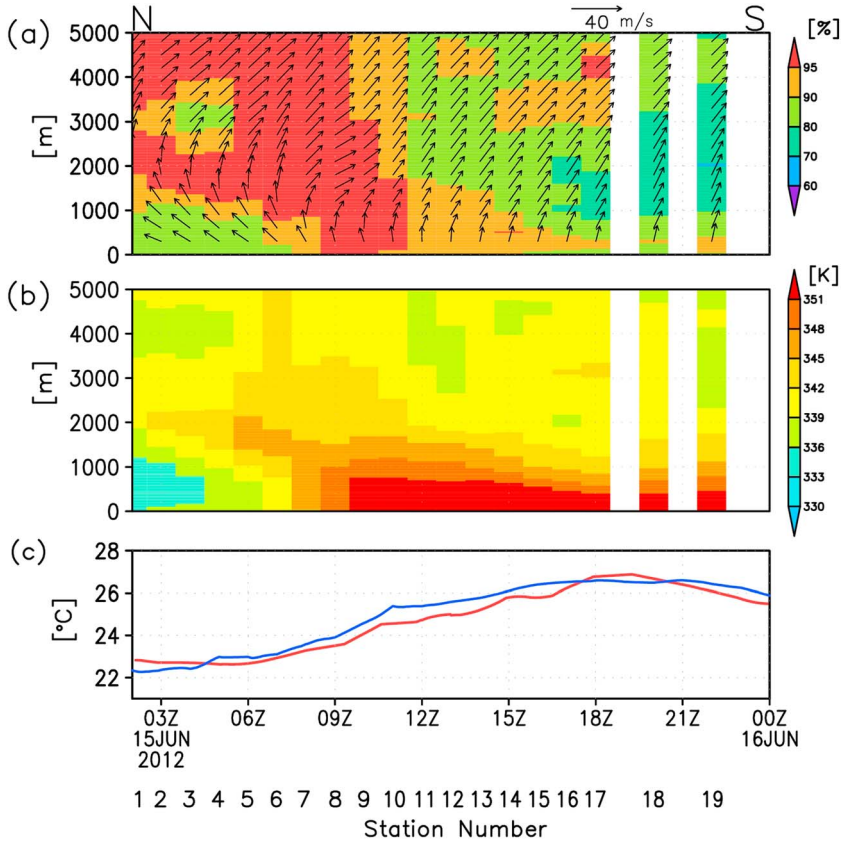

Figure 6. Atmospheric and oceanic fields obtained by virtual samplings using M-ANAL data. (a) Time-height cross sections of relative humidity (color) in percent and horizontal wind (vector). Vectors directed downward denote northerlies. (b) Equivalent potential temperature in Kelvin. (c) Time series of SST (red) and SAT (blue) in degree Celcius. All the data were sampled at same locations and times as those of field campaign.

4. Frontal Structures

This section describes the detailed frontal structures during the field campaign. Figure 5 displays observations along the sounding transect. The southwesterly flow is dominant at heights above 3000 m, which is consistent with GSM data (Figure 2). In the lower troposphere (surface to 1000 m elevation), southerlies with warm and humid air prevailed south of station 10. The southerlies correspond to the prefrontal warm moist southerly flow as displayed in Figure 3.

Between sounding stations 6 and 7, wind direction changed rapidly from southeasterlies to southwesterlies in the lower troposphere (Figure 5a), accompanied by a steep rise of SAT (Figure 5c). The frontal structure characterized by these changes of wind direction and SAT between stations 6 and 7 is referred to as the "northern atmospheric front" in the rest of this paper. The wind direction changed in the layer between 1000 m and 2000 m over the northern atmospheric front and dry air appeared over the front, consistent with the conceptual model proposed by *Kato et al.* [2003]. The wind direction changed again at around 2000 m.

Similar to the northern atmospheric front, the lower atmosphere between stations 9 and 10 experienced a rapid change of wind direction and SAT increase. The frontal structure between stations 9 and 10 is henceforth referred to as the "southern atmospheric front." Because these changes occur between stations 9 and 10 when the ship moves across the southern edge of the convective line (Figures 4i and 4j), these features could be due to the gust front or outflow boundary at the leading of the convective line.

Two steep SST rises were recorded (Figure 5c). One was between stations 6 and 7 (henceforth referred to as "northern oceanic front"), and the other between stations 16 and 17. Time changes in MGDSST from 15 to 16 June

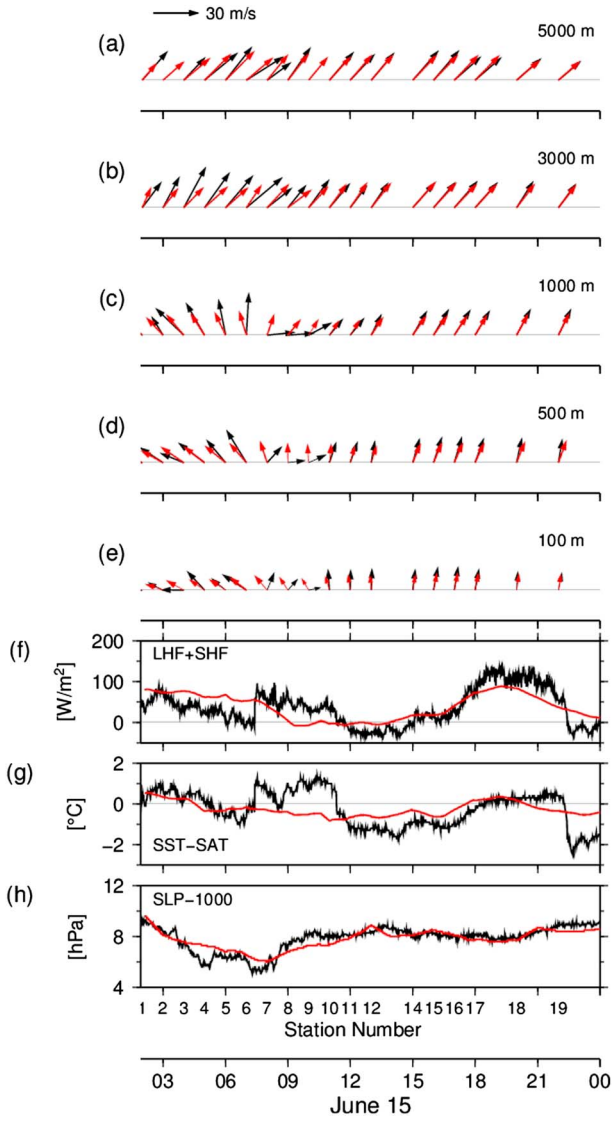

Figure 7. Time series of the near surface static stability, turbulent heat flux, and the vertical structure of the wind fields. In-situ and M-ANAL data are indicated by black and red lines (vectors), respectively. Time series of the wind vectors at heights of (a) 5000 m, (b) 3000 m, (c) 1000 m, (d) 500m, (e) 100 m, (f) sum of the latent sensible heat fluxes, (g) differences between SST and SAT, and (h) SLP-1000.

were small (not shown), as expected from the large heat capacity of the ocean. Therefore, the two SST increases were not attributable to rapid SST time changes but likely to the SST fronts. SST further rose to a maximum south of station 17 during the campaign and maintained its highest value (~27°C) between stations 17 and 19, and decreased rapidly south of station 19. Consistently, subsurface water temperature between stations 17 and 18 was warmer than 26°C to a depth 60 m (Figure 5d). The location of this warm water is consistent with the warm tongue extended northeastward between the continental shelf and the Ryukyu Islands (Figure 1), indicative of the Kuroshio in the ECS [*Xie et al.*, 2002]. We thus refer to this warm water between stations 17 and 18 as Kuroshio water. The northern oceanic front was ~100 km north of the Kuroshio water. This oceanic front is probably due to the tongue of warm water extending from the Kuroshio. This tongue is a prominent feature in the northeastern ECS [*Huh*, 1982; *Qiu et al.*, 1990; *Manda et al.*, 2000]. In summary, the field campaign captured the two frontal structures in the lower atmosphere, characterized by rapid changes of wind direction and SAT, and two prominent features of the SST field, i.e., the northern oceanic front and warm Kuroshio water.

In order to complement the in situ data, the atmospheric and oceanic fields of M-ANAL data are virtually sampled using bilinear interpolation in space and linear interpolation in time (Figure 6). Southwesterlies dominated at heights above 3000 m were well reproduced. Moreover, the lower-layer warm and humid air (EPT $>$ 350 K) and southerly flow were also well reproduced south of the southern atmospheric front. However, the features extended further north than observed. The rapid changes of wind direction around the northern and southern atmospheric fronts were not obvious in the M-ANAL. MGDSST that is used in the M-ANAL system does not well reproduce the complex SST field north of station 11, including northern oceanic front (Figure 6c). These discrepancies will be further explored in association with the impact of the SST field on the atmosphere in the next section.

5. Oceanic Influences on the BFZ

As described in the introduction section, recent studies indicate the impacts of SST on the atmosphere in the mid latitudes. The readers are referred to references given in section 1 and a comprehensive review by *Small et al.* [2008]. Some significant features of SST were observed during our field campaign, such as the warm Kuroshio

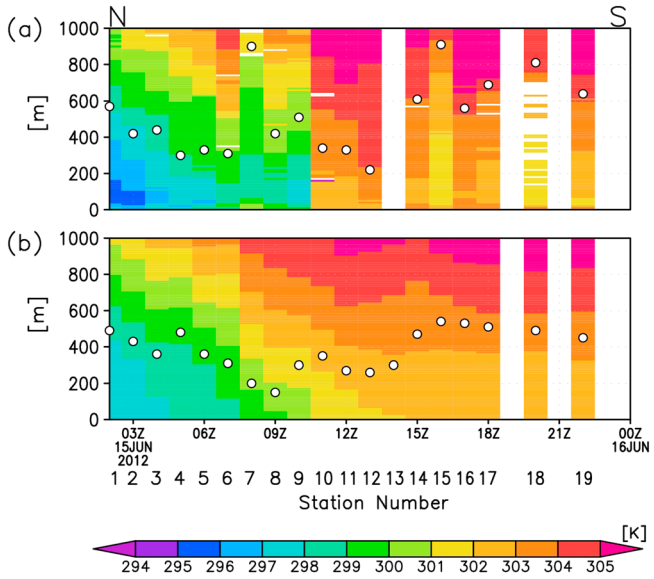

Figure 8. Time-height sections of virtual potential temperature of (a) in situ and (b) M-ANAL data. Open circles denote the MABL height defined as the lowest height where virtual potential temperature increases by 1°C from the sea surface.

water in which SST exceeds 27°C and abrupt SST changes north of station 11 (Figure 5c). As indicated by these studies, it is likely these features exert an impact on the atmosphere, which will be discussed in this section.

5.1. Influence of SST on the MABL in the BFZ

As described in the last section, while the ship was traveling between stations 5 and 8, wind in the layer between the sea surface and 1000 m veered in time approximately 110°. Concurrently, shipboard SST exhibits steep rise of 3°C (Figure 5c). Such SST rise has a potential impact to change the MABL structure. To elaborate the relationship between these wind change and SST fields, we compare the in situ measurements with M-ANAL data in Figure 7. In the middle troposphere (3000 and 5000 height levels) throughout the period of the field campaign, the prevailing winds were southwesterlies, which was reproduced well in M-ANAL. At the stations south of southern atmospheric front (south of station 10), the southerlies in the lower troposphere (from 100 to 1000 m height levels) were also reproduced well in M-ANAL. However, at the stations between stations 7 to 10, the vertical structures of the in situ wind vary significantly in the lower troposphere (from 100 to 1000 m height levels), which are not reproduced in the M-ANAL data. Figure 8 displays time-height sections of virtual potential temperature along with the MABL height, which is one of the key parameters to inspect whether the SST influences the stability of the lower troposphere [*Tokinaga et al.*, 2006]. In this study, the MABL height is defined as the lowest height where virtual potential temperature increases by 1 °C from the sea surface [*Tokinaga et al.*, 2006]. The MABL of in situ data is thicker than that of MSM data at the stations south of the northern atmospheric front (stations 7–10) and around the Kuroshio water (stations 14–19), indicating in situ data exhibit lower stability than MSM data in the lower troposphere at these stations. The near surface static stability evaluated by the difference in SST and SAT exhibits unstable condition between stations 7 and 9 only in the in situ data (Figure 7g). In contrast, M-ANAL shows stable conditions at these stations. At these stations, the upward turbulent heat flux estimated by in situ data intensifies and exhibits a sharp contrast compared to the stations north of station 7 and south of station 10. M-ANAL data, however, do not show such a sharp contrast of the heat flux. The near surface unstable conditions and intensified heat flux lead to a decrease of atmospheric stability in the lower troposphere.

There are two primary mechanisms for sea surface wind response to SST fronts: vertical mixing and SST front–induced sea level pressure adjustment mechanisms. In the vertical mixing mechanism, warm (cold) SST weakens (strengthens) the near-surface static stability and thereby enhances (reduces) vertical mixing in the MABL [*Wallace et al.,* 1989]. *Lindzen and Nigam* [1987] proposed the pressure adjustment mechanisms that sea level pressure (SLP) adjusts to an SST front through the changes in the MABL temperature field. In this mechanism, SST generates a difference of air temperature in the MABL across a front, and the resultant pressure anomalies produce wind convergence over bands of warm SST, which sometimes induces deep convection [*Minobe et al.*, 2008, 2010; *Back and Bretherton*, 2009; *Li and Carbone*, 2012]. As well as the pressure adjustment mechanism, recent studies indicate the vertical mixing mechanism works in the East China Sea during spring and early summer [*Xu et al.*, 2011; *Liu et al.,* 2013]. The analysis shown here is supportive of the vertical mixing mechanism. Interestingly, a recent diagnostic study using the result of numerical experiments indicates that the pressure adjustment and vertical mixing mechanisms are not exclusive. They coexist and work simultaneously [*Takatama et al.*, 2011]. In fact, SLP decreases around the northern atmospheric

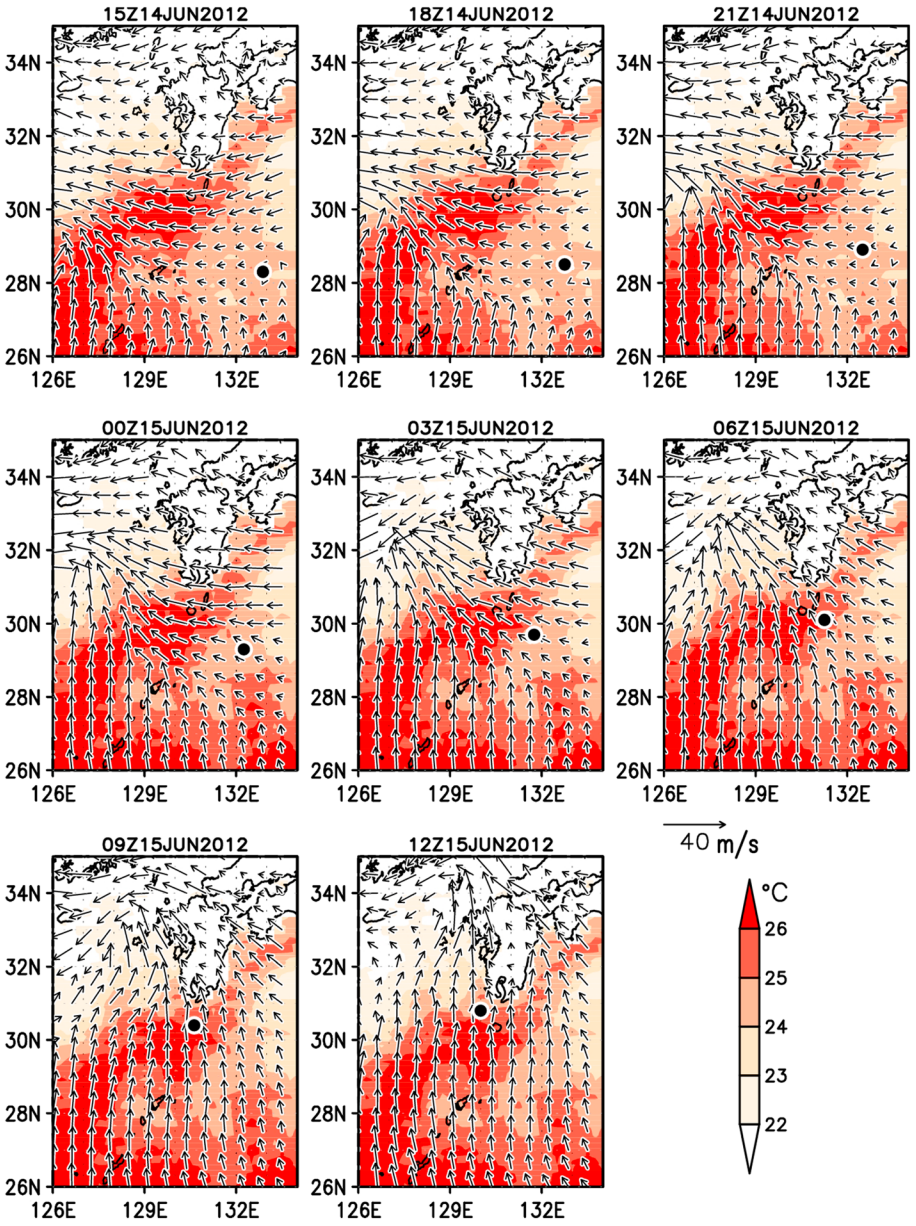

Figure 9. Backward trajectory of air parcel released at the location of station 11 at 1200 UTC on 15 June at 975 hPa level (solid circles), overlaying horizontal wind vectors of M-ANAL and color shadings representing MGDSST.

front (Figure 7h), which is consistent with the pressure adjustment mechanism. In order to further examine whether the pressure adjustment mechanism surely works, we need to check the relationship between SST and SLP Laplacians, which cannot be computed from the in situ data obtained during the field campaign. Unfortunately, the SST structure around the northern oceanic front is not reproduced well in the currently available SST data sets such as MGDSST (Figure 6c) and JCOPE2 (not shown), which means definitive conclusions using these data are not possible.

5.2. Influence of Moisture Supply From the Kuroshio on the BFZ

The importance of moisture transport in the ECS to BFZ has been well recognized [e.g., *Ogura et al.*, 1985; *Kato*, 1998]. However, the role of SST has not been fully examined, except in a few recent studies [e.g., *Sasaki et al.*, 2012; *Tsuguti and Kato*, 2014; *Manda et al.*, 2014]. As shown in Figure 7f, turbulent heat flux reached its maximum observed during the cruise in excess of 150 W m^{-2} over the Kuroshio water. Since the latent heat

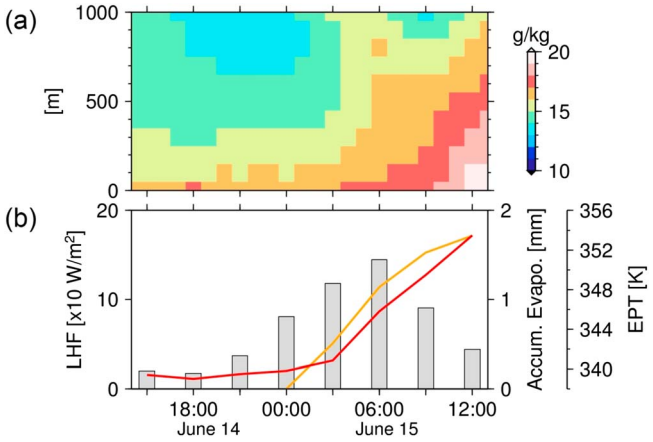

Figure 10. (a) Time-height diagram of the water vapor mixing ratio, sampled at times and locations of the air parcel. (b) Time histories of latent heat flux in W m^{-2} (bar) along the backward trajectory and accumulated evaporation in mm (orange line) after air parcel traversed Kuroshio water, and the EPT of the air parcel (red line).

flux dominated turbulent heat flux (not shown), this result indicates the intensive evaporation and thus moisture supply over the Kuroshio water. However, EPT near the sea surface reached its maximum not just above but north of the Kuroshio water, i.e., around stations 11 (Figure 5b). The southerlies dominated south of southern atmospheric front in the lower troposphere (Figures 5a and 7e). These results suggest the meridional moisture transport from the high SST region to the Baiu front, as reported by *Tanimoto et al.* [2009]. *Tsuguti and Kato* [2014] recently showed the importance of remote moisture supply from a high SST area to a mesoscale convective system in a maritime region. To illustrate moisture transport processes during the sounding campaign, we performed a back-trajectory analysis and evaluated the contribution of evaporation over the Kuroshio water to the water vapor content and stability in the lower troposphere.

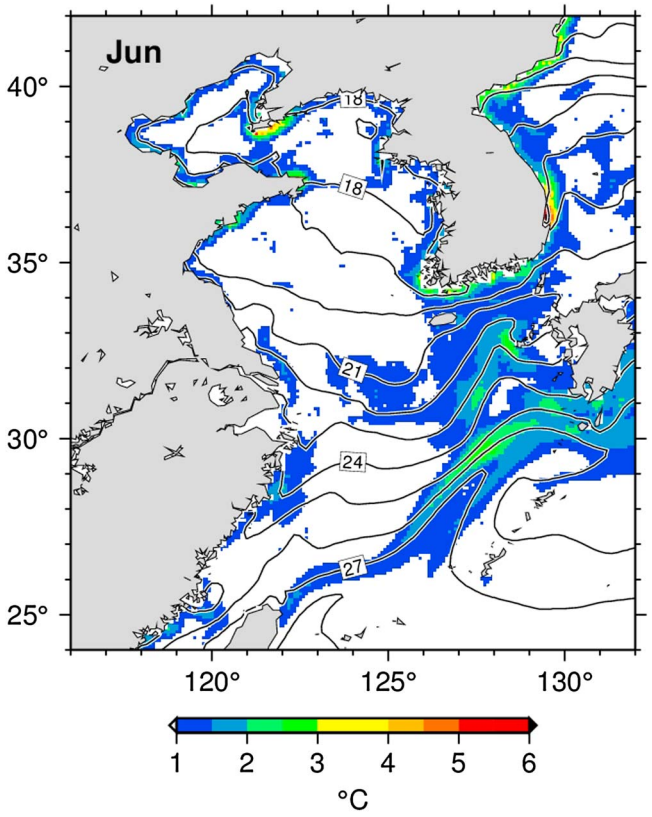

Figure 11. Map of monthly mean SST (contour) and standard deviation from its monthly mean (color) in June (°C), computed from daily JCOPE2 reanalysis data of 2000–2009.

In the back-trajectory analysis, we used M-ANAL for atmospheric data and MGDSST, which is used in M-ANAL, for SST data. As mentioned above, M-ANAL reproduced well the lower-layer southerly flow south of the southern atmospheric front, and MGDSST represents the overall SST trend in the shipboard records south of the southern atmospheric front. Figure 9 displays the backward trajectory of an air parcel released at 1200 UTC on 15 June 2012 at the 975 hPa level above station 11 [31.0°N, 130.0°E]. This location was south of the southern atmospheric front and where the ship was north of the Kuroshio water. Dots indicate locations of the parcel. The southerly flow transported the air parcel from south of the Japanese Islands [28.3°N, 132.9°E] to station 11 in ~21 h. Intense evaporation over the Kuroshio water may have supplied water vapor while the parcel traversed this water from 0300 to 0900 UTC on 15 June. The time history of latent heat flux and accumulated evaporation along the back trajectory, and the EPT of the air

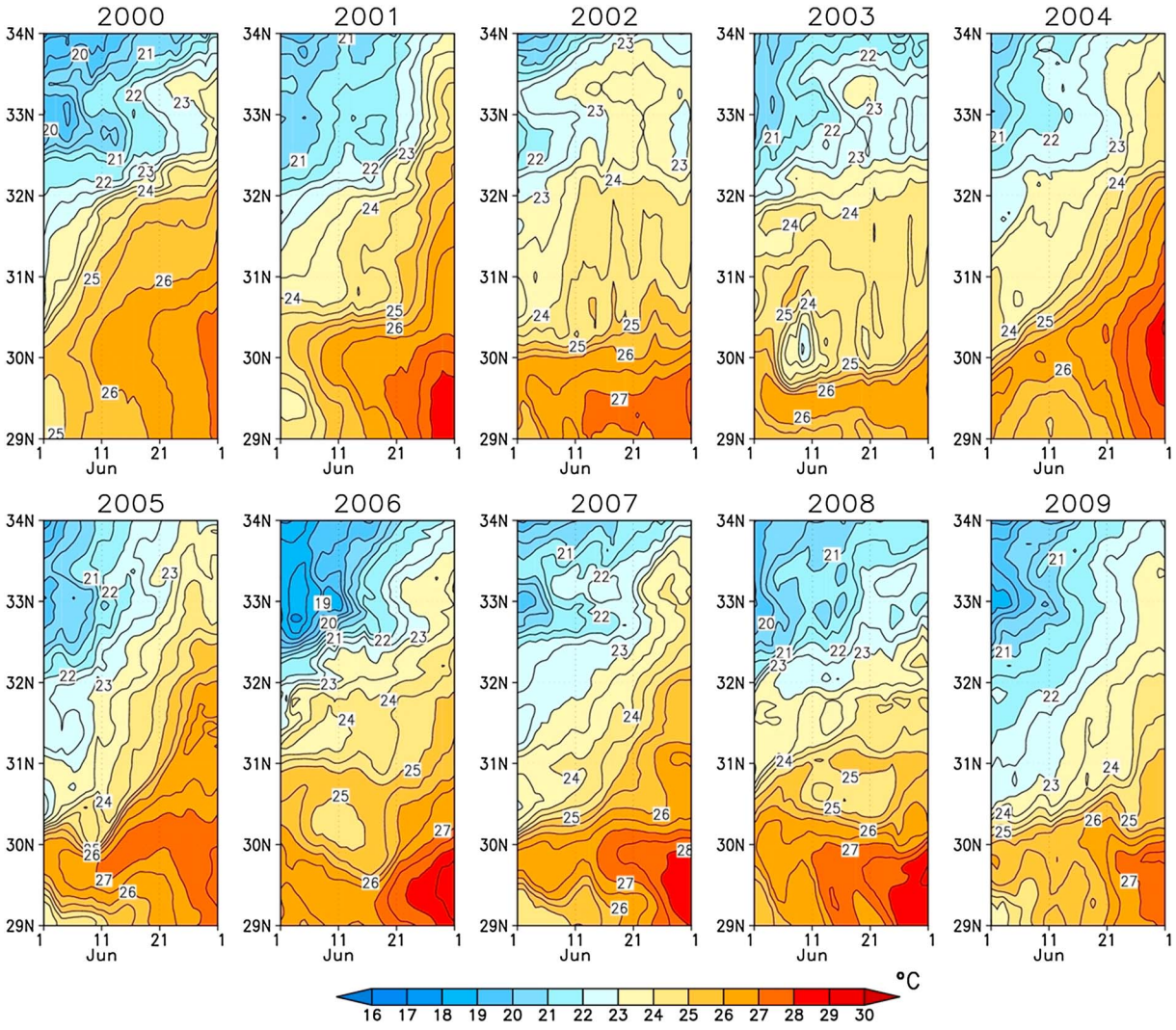

Figure 12. Time-latitude sections of daily JCOPE2 SST along 128.5°E in June, from 2000 and 2009.

parcel, were thus estimated to quantify the influence of the Kuroshio water (Figure 10). The meteorological data of M-ANAL and MGDSST at locations of the air parcel were sampled by using bilinear interpolation in space and linear interpolation in time, and the latent heat flux was estimated by bulk aerodynamic formula [*Kondo*, 1975].

Latent heat flux exceeded 100 W m^{-2} from 0600 to 0900 UTC on 15 June when the air parcel traversed the Kuroshio water. The increase in accumulated evaporation corresponds well with increase in the water vapor mixing ratio in the lower troposphere (Figure 10). EPT of the air parcel also increased along with accumulated evaporation. These results indicate the importance of the moisture supply over the Kuroshio in the water vapor content and stability in the lower troposphere of the BFZ.

The analysis shown here indicates the importance of a remote influence of moisture transport from a high SST region where intense evaporation has raised air mass water vapor content. MGDSST underestimated in situ SST over the Kuroshio water, which leads to the underestimation of evaporation. This indicates that the evaporation over the Kuroshio water is more important than estimated here. This result also suggests that the quality of SST data used in numerical models affects moisture budgets and atmospheric stability in the lower troposphere. They are important factors for forecasting the precipitation system of the BFZ. Continuous monitoring of oceanic conditions is highly desirable for improving forecast skill.

6. Summary and Discussion

The intensive sounding campaign in the ECS was conducted during June 2012 to investigate the influence of the SST field on frontal structures of the BFZ. Two distinct frontal structures were observed during the sounding campaign. The northern atmospheric front observed between stations 6 and 7 was accompanied by changes of wind direction, SAT, and SST (Figure 4a). Relatively high SST south of the northern atmospheric front enhanced near surface unstable condition and intensified turbulent heat flux. They help modify the MABL structure in the BFZ. Since the detailed SST distributions observed in shipboard data were not well reproduced in satellite SST data used in this study, the detailed mechanisms of the wind changes in the MABL have not been clarified, but this issue should be explored in future studies. The southern atmospheric front observed between stations 9 and 10 was characterized by a change of wind direction and SAT. The front was south of the precipitation system and is considered the southern end of the BFZ. Intense evaporation over the Kuroshio water and moisture transport from it to the southern atmospheric front are important contributors to water vapor content and stability in the lower troposphere of the BFZ.

Although the Baiu front is depicted as a stationary front on operational weather charts, the BFZ has strong variations in space and time [e.g., *Ninomiya,* 1984; *Ninomiya and Akiyama*, 1992; *Ninomiya and Shibagaki*, 2007; *Moteki et al.,* 2004a, 2004b, 2006; *Maeda et al.*, 2008; *Moteki and Manda*, 2013]. The SST field in the northeastern ECS also exhibits large spatiotemporal variations. Standard deviation of SST from its monthly mean is large in the northeastern ECS during June (Figure 11). In fact, SST fields vary significantly in atmospheric subsynoptic time scale in that region, in addition to having strong interannual variation (Figure 12). These variations may affect the BFZ. The relationship between the variations in the BFZ and those of SST should be an important subject in future studies for understanding mechanisms of the BFZ variations.

Acknowledgments

The authors wish to thank the crews of T/V *Nagasaki-Maru* and participants in the field campaign. We also would like to thank Y. Kawai of JAMSTEC, Japan for his support, without which this study would not have been possible. Our thanks are extended to Y. Miyazawa and R. Zhang of JAMSTEC for providing the JCOPE2 data and their assistance. M-ANAL analyses, GSM outputs, and radar precipitation data were provided by the JMA and distributed by the Research Institute for Sustainable Humanosphere, Kyoto University (http://database.rish.kyoto-u.ac.jp/arch/jmadata/). MGDSST data are available at http://goos.kishou.go.jp/. The MTSAT-2 satellite images are provided by Kochi University (http://weather.is.kochi-u.ac.jp/) and JMA. This work was supported in part by the Japan Society for Promotion for Science (JSPS) through a Grant-in-Aid for Scientific Research (22244057) and by the Japanese Ministry of Education, Culture, Sports, Science, and Technology (MEXT) through a Grant-in-Aid for Scientific Research on Innovative Areas 2205 (22106003).

References

Akiyama, T. (1973), The large-scale aspect of the characteristic features of the Baiu front, *Paper. Meteorol. Geophys.*, *24*(2), 157–188.

Back, L. E., and C. S. Bretherton (2009), On the relationship between SST gradients, boundary layer winds, and convergence over the tropical oceans, *J. Clim.*, *22*(15), 4182–4196, doi:10.1175/2009JCLI2392.1.

Chen, T.-J. G., and C.-P. Chang (1980), The Structure and vorticity budget of an early summer monsoon trough (Mei-Yu) over southeastern China and Japan, *Mon. Weather Rev.*, *108*(7), 942–953, doi:10.1175/1520-0493(1980)108<0942:TSAVBO>2.0.CO;2.

Davidson, N. E., K. Kurihara, T. Kato, G. Mills, and K. Puri (1998), Dynamics and prediction of a mesoscale extreme rain event in the Baiu front over Kyushu, Japan, *Mon. Weather Rev.*, *126*(6), 1608–1629, doi:10.1175/1520-0493(1998)126<1608:DAPOAM>2.0.CO;2.

Ding, Y., and J. C. L. Chen (2005), The East Asian summer monsoon: An overview, *Meteorol. Atmos. Phys.*, *89*, 117–142, doi:10.1007/s00703-005-0125-z.

Huh, O. (1982), Spring season flow of the Tsushima Current and its separation from the Kuroshio: Satellite evidence, *J. Geophys. Res.*, *87*(C12), 9687–9693, doi:10.1029/JC087iC12p09687.

Kato, T. (1998), Numerical simulation of the band-shaped torrential rain observed over southern Kyushu, Japan on 1 August 1993, *J. Meteorol. Soc. Jpn.*, *76*(1), 97–128.

Kato, T., M. Yoshizaki, K. Bessho, T. Inoue, Y. Sato, and X-BAIU-01 observation group (2003), Reason for the failure of the simulation of heavy rainfall during X-BAIU-01—Importance of a vertical profile of water vapor for numerical simulations, *J. Meteorol. Soc. Jpn.*, *81*(5), 993–1013, doi:10.2151/jmsj.81.993.

Kodama, Y.-M. (1992), Large-scale common features of subtropical precipitation zones (the Baiu frontal zone, the SPCZ, and the SACZ). Part I: Characteristics of subtropical frontal zones, *J. Meteorol. Soc. Jpn.*, *70*(4), 813–836.

Kondo, J. (1975), Air-sea bulk transfer coefficients in diabatic conditions, *Bound. Layer Meteor.*, *9*(1), 91–112, doi:10.1007/BF00232256.

Kushnir, Y., W. A. Robinson, I. Bladé, N. M. J. Hall, S. Peng, and R. Sutton (2002), Atmospheric GCM response to extratropical SST anomalies: Synthesis and evaluation, *J. Clim.*, *15*(16), 2233–2256, doi:10.1175/1520-0442(2002)015<2233:AGRTES>2.0.CO;2.

Kuwano-Yoshida, A., B. Taguchi, and S.-P. Xie (2013), Baiu rainband termination in atmospheric and coupled atmosphere–ocean models, *J. Clim.*, *26*(24), 10,111–10,124, doi:10.1175/JCLI-D-13-00231.1.

Li, Y., and R. E. Carbone (2012), Excitation of rainfall over the tropical western Pacific, *J. Atmos. Sci.*, *69*(10), 2983–2994, doi:10.1175/JAS-D-11-0245.1.

Lindzen, R. S., and S. Nigam (1987), On the role of sea surface temperature gradients in forcing low level winds and convergence in the tropics, *J. Atmos. Sci.*, *44*(17), 2418–2436, doi:10.1175/1520-0469(1987)044<2418:OTROSS>2.0.CO;2.

Liu, J.-W., S.-P. Zhang, and S.-P. Xie (2013), Two types of surface wind response to the East China Sea Kuroshio Front, *J. Clim.*, *26*(21), 8616–8627, doi:10.1175/JCLI-D-12-00092.1.

Maeda, S., K. Tsuboki, Q. Moteki, T. Shinoda, H. Minda, and H. Uyeda (2008), Detailed structure of wind and moisture fields around the Baiu frontal zone over the East China Sea, *SOLA*, *4*, 141–144, doi:10.2151/sola.2008-036.

Manda, A., A. Isobe, K. Omura, and Y. Kyozuka (2000), Low-frequency temperature variability at Fukue Island located southwest of the Tsushima Straits, *J. Oceanogr.*, *56*(2), 141–152.

Manda, A., H. Nakamura, N. Asano, S. Iizuka, T. Miyama, Q. Moteki, M. K. Yoshioka, K. Nishii, and T. Miyasaka (2014), Impacts of a warming marginal sea on torrential rainfall organized under the Asian summer monsoon, *Sci. Rep.*, *4*, doi:10.1038/srep05741.

Minobe, S., A. Kuwano-Yoshida, N. Komori, S.-P. Xie, and R. J. Small (2008), Influence of the Gulf Stream on the troposphere, *Nature*, *452*, 206–209, doi:10.1038/nature06690.

Minobe, S., M. Miyashita, A. Kuwano-Yoshida, H. Tokinaga, and S.-P. Xie (2010), Atmospheric response to the Gulf Stream: Seasonal variations, *J. Clim.*, *23*(13), 3699–3719, doi:10.1175/2010JCLI3359.1.

Minobe, S., et al. (2015), Air-sea interaction over the western boundary currents in the western North Pacific, in *Indo-Pacific Climate Variability and Predictability, World Scientific Series on Asia-Pacific Weather and Climate*, vol. *7*, edited by T. Yamagata and S. Behera, World Scientific, Singapore, in press.

Miyama, T., M. Nonaka, H. Nakamura, and A. Kuwano-Yoshida (2012), A striking early-summer event of a convective rainband persistent along the warm Kuroshio in the East China Sea, *Tellus A*, *64*, 18962, doi:10.3402/tellusa.v64i0.18962.

Miyazawa, Y., R. Zhang, X. Guo, H. Tamura, D. Ambe, J.-S. Lee, A. Okuno, H. Yoshinari, T. Setou, and K. Komatsu (2009), Water mass variability in the western North Pacific detected in a 15-year eddy resolving ocean reanalysis, *J. Oceanogr.*, *65*(6), 737–756, doi:10.1007/s10872-009-0063-3.

Moteki, Q., and A. Manda (2013), Seasonal migration of the Baiu frontal zone over the East China Sea: Sea surface temperature effect, *SOLA*, *9*, 19–22, doi:10.2151/sola.2013-005.

Moteki, Q., H. Uyeda, T. Maesaka, T. Shinoda, M. Yoshiozaki, and T. Kato (2004a), Structure and development of two merged rainbands observed over the East China Sea during X-BAIU-99, Part I: Meso scale structure and development processes, *J. Meteorol. Soc. Jpn.*, *82*(1), 19–44, doi:10.2151/jmsj.82.19.

Moteki, Q., H. Uyeda, T. Maesaka, T. Shinoda, M. Yoshiozaki, and T. Kato (2004b), Structure and development of two merged rainbands observed over the East China Sea during X-BAIU-99, Part II: Meso scale structure and development processes, *J. Meteorol. Soc. Jpn.*, *82*(1), 45–65, doi:10.2151/jmsj.82.45.

Moteki, Q., T. Shinoda, S. Shimizu, S. Maeda, H. Minda, K. Tsuboki, and H. Uyeda (2006), Multiple frontal structures in the Baiu frontal zone observed by aircraft on 27 June 2004, *SOLA*, *2*, 132–135, doi:10.2151/sola.2006-034.

Ninomiya, K. (1984), Characteristics of Baiu front as a predominant subtropical front in the summer Northern Hemisphere, *J. Meteorol. Soc. Jpn.*, *62*(6), 880–894.

Ninomiya, K., and T. Akiyama (1992), Multi-scale features of Baiu, the summer monsoon over Japan and East Asia, *J. Meteorol. Soc. Jpn.*, *70*(1B), 467–495.

Ninomiya, K., and Y. Shibagaki (2007), Multi-scale features of the Meiyu-Baiu front and associated precipitation systems, *J. Meteorol. Soc. Jpn.*, *85B*, 103–122, doi:10.2151/jmsj.85B.103.

Ogura, Y., T. Asai, and K. Dohi (1985), A case study of a heavy precipitation event along the Baiu front in northern Kyushu, 23 July 1982: Nagasaki heavy rainfall, *J. Meteorol. Soc. Jpn.*, *63*(5), 883–900.

Qiu, B., T. Toda, and N. Imasato (1990), On Kuroshio front fluctuations in the East China Sea using satellite and in situ observational data, *J. Geophys. Res.*, *95*(C10), 18,191–18,204, doi:10.1029/JC095iC10p18191.

Sampe, T., and S.-P. Xie (2010), Large-scale dynamics of the Meiyu-Baiu rainband: Environmental forcing by the westerly jet, *J. Clim.*, *23*(1), 113–134, doi:10.1175/2009JCLI3128.1.

Sasaki, Y. N., S. Minobe, T. Asao, and M. Inatsu (2012), Influence of the Kuroshio in the East China Sea on the early summer (Baiu) rain, *J. Clim.*, *25*(19), 6627–6645, doi:10.1175/JCLI-D-11-00727.1.

Small, R. J., S. P. deSzoeke, S.-P. Xie, L. O'Neill, H. Seo, Q. Song, P. Cornillon, M. Spall, and S. Minobe (2008), Air–sea interaction over ocean fronts and eddies, *Dynam. Atmos. Oceans*, *45*(3–4), 274–319, doi:10.1016/j.dynatmoce.2008.01.001.

Takatama, K., S. Minobe, M. Inatsu, and R. J. Small (2011), Diagnostics for near-surface wind convergence/divergence response to the Gulf Stream in a regional atmospheric model, *Atmos. Sci. Lett.*, *13*(1), 16–21, doi:10.1002/asl.355.

Tanimoto, Y., S.-P. Xie, K. Kai, H. Okajima, H. Tokinaga, T. Murayama, M. Nonaka, and H. Nakamura (2009), Observation on marine atmospheric boundary layer transitions across the summer Kuroshio Extension, *J. Clim.*, *22*(6), 1360–1374, doi:10.1175/2008JCLI2420.1.

Tokinaga, H., Y. Tanimoto, M. Nonaka, B. Taguchi, T. Fukamachi, S.-P. Xie, H. Nakamura, T. Watanabe, and I. Yasuda (2006), Atmospheric sounding over the winter Kuroshio Extension: Effect of surface stability on atmospheric boundary layer structure, *Geophys. Res. Lett.*, *33*, L04703, doi:10.1029/2005GL025102.

Tsuguti, H., and T. Kato (2014), Contributing factors of the heavy rainfall event at Amami-Oshima Island, Japan, on 20 October 2010, *J. Meteorol. Soc. Jpn.*, *92*(2), 163–183, doi:10.2151/jmsj.2014-202.

Wallace, J. M., T. P. Mitchell, and C. Deser (1989), The influence of sea-surface temperature on surface wind in the eastern Equatorial Pacific: Seasonal and interannual variability, *J. Clim.*, *2*(12), 1492–1499, doi:10.1175/1520-0442(1989)002<1492:TIOSST>2.0.CO;2.

Xie, S.-P., J. Hafner, Y. Tanimoto, W. T. Liu, H. Tokinaga, and H. Xu (2002), Bathymetric effect on the winter sea surface temperature and climate of the Yellow and East China Seas, *Geophys. Res. Lett.*, *29*(24), 2228, doi:10.1029/2002GL015884.

Xu, H., M. Xu, S.-P. Xie, and Y. Wang (2011), Deep atmospheric response to the spring Kuroshio over the East China Sea, *J. Clim.*, *24*(18), 4959–4972, doi:10.1175/JCLI-D-10-05034.1.